Exploring the carbon nanocosmos: doped nanotubes, networks, and other novel forms of carbon

M. Terrones* [a], P.M. Ajayan [b], F. Banhart [c], X. Blase [d], D.L. Carroll [e], J.C. Charlier [f], R. Czerw [e], N. Grobert [g], R. Kamalakaran [g], M. Mayne [h], M. Reyes-Reyes [a], M. Rühle [g], T. Seeger [g], H. Terrones [a]

[a] *Advanced Materials Department, IPICyT, Venustiano Carranza 2425-A, Col. Los Filtros, 78210 San Luis Potosí, SLP. México*

[b] *Department of Materials Science & Engineering, Rensselaer Polytechnic Institute, NY-USA*

[c] *Z.E. Elektronenmikroskopie, Universität Ulm, 89069 Ulm, Germany*

[d] *Département de Physique des Matériaux, Université Claude Bernard, 69622 Villeurbanne, France*

[e] *Department of Physics and Astronomy, Clemson University, Clemson SC 29634, USA*

[f] *Unit of Physics of Materials (PCPM), University of Louvain, 1348 Louvain-la-Neuve, Belgium*

[g] *Max-Planck-Institut fuer Metallforschung, Heisenbergstrasse 3, D-70569 Stuttgart, Germany*

[h] *Laboratoire Francis Perrin CEA-CNRS URA2453, CEA Saclay - ВГт.522, 9119, France*

Abstract

High temperature routes to arrays of aligned CN_x nanotubes and B-doped carbon nanotubes are presented. The materials have been characterized using state-of-the-art techniques such as high-resolution electron energy loss spectroscopy (HREELS), scanning tunneling spectroscopy (STS) and high-resolution transmission electron microscopy (HRTEM). Using STS, we show that the doped nanotubes exhibit strong features on the conduction (for CN_x nanotubes) and valence band (for B-doped nanotuebs) close to the Fermi level, thus indicating that electron-rich (CN_x) and hole-rich (B-doped) nanotubes are indeed fabricated (n- and p-type respectively). Tight-binding and ab-inito calculations confirm our experimental results obtained using STS. Finally, it is demonstrated that high electron irradiation at 700 – 800 °C, is capable of creating "X" and "Y" junctions using single-walled nanotubes (SWNTs). The process has also been studied using tight-binding molecular dynamics (TBMD). Vacancies trigger the organization of atoms on the tube lattices within adjacent tubes. These results pave the way to the fabrication of nanotube heterojunction networks, robust composites, contacts, nanocircuits and strong 3D composites.

Nanotechnology, Robert Vajtai, Xavier Aymerich, Laszlo B. Kish, Angel Rubio, Editors,
Proceedings of SPIE Vol. 5118 (2003) © 2003 SPIE · 0277-786X/03/$15.00

1. Introduction

Following the discovery of C_{60}:Buckminsterfullerene by Kroto, et al. [1], the development of a new field involving carbon nanostructures rapidly emerged. As a result, in 1991, closed and elongated tubular carbon structures (also termed carbon nanotubes) were identified [2-3]. Carbon nanotubes are now produced using the arc discharge [4], thermolysis of hydrocarbons over catalysts [4-7], laser vaporization of graphite [4,8], and by electrolysis of ionic salts using graphite electrodes [9].

In addition, carbon nanotubes possess extremely high Young modulus and can behave as metals or semiconductors depending upon chirality and diameter [10]. Recent examples of nanotube applications [10-12] include use of nanotubes as: (i) gas storage components for Ar, N_2 and H_2; (ii) STM probes and field emission sources; (iii) high power electrochemical capacitors; (iv) chemical sensors; (v) electronic nanoswitches; (vi) magnetic storage devices (*e.g.* Fe-filled nanotubes), etc [10-12].

In this account, the production, structure and characterization of CN_x and B-doped carbon nanotubes are presented. CN_x nanotubes are mainly prepared by pyrolysis of organometallic precursors such as ferrocene (biscyclopentadynil-Iron) in conjunction with N-containing precursors (e.g. melamine –triaminotriazine, pyridene, *etc.*). For B-doped carbon nanotubes arc discharge methods are used. The electronic properties of these doped tubular structures have been studied using STS, and the results have been confirmed experimentally using first principles and tight binding calculations.

Little progress has been reported on techniques related to connect nanotubes so that novel devices are produced. Theory predicts that a "Y" or a "T" junction could act as multi-terminal electronic device involving SWNTs [13-18]. In this account, we also demonstrate that controlled electron beam exposure at elevated temperatures, is capable of connecting SWNTs, thus forming "X", "T" and "Y" junctions. We investigate the process at the atomic level using TBMD calculations, which revealed that vacancies and interstitials, formed under controlled electron beam doses, trigger the formation of molecular connections.

2. CN_x nanotubes

Pyrolytic self-assembly processes were used to fabricate large arrays (< 400x400 μm^2) of aligned C_9N_x ($x \leq 1$) nanofibers (< 100 nm OD, 60 μm length) in a single step process: *e.g.* the thermolysis of ferrocene/melamine mixtures at 950-1050 °C under an Ar atmosphere, (Fig. 1) [19]. The overall morphology exhibits a carpet-like structure, in which the C/N nanotubes constitute the pile.

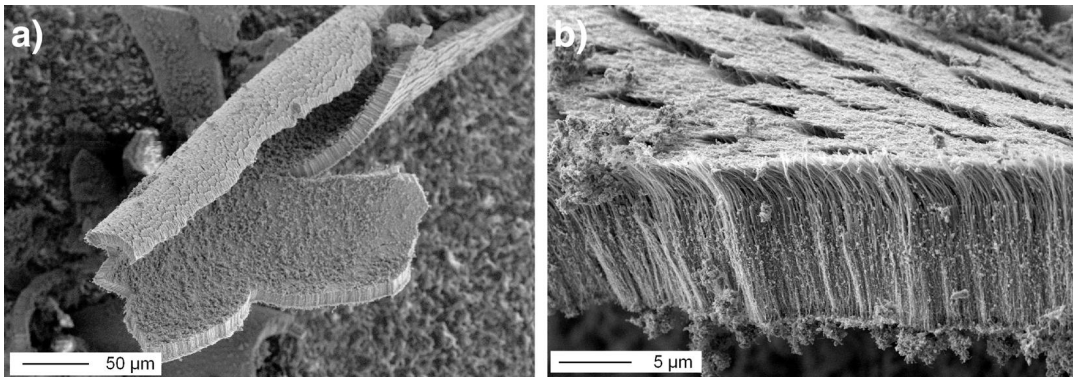

FIGURE 1. SEM images of: (a) a large flake (top view) containing aligned CN_x nanofibers; (b) higher magnification of a flake exhibiting densely packed fibers of uniform diameter (< 60nm OD).

HRTEM and HREELS studies reveal that: (a) the hollow nanofibers possess unusual irregular stacked-cone corrugated morphologies, and (b) the degree of tubular perfection decreases as a result of the nitrogen incorporation (Fig. 2). EEL spectra of the nanofibers revealed the presence of ionization edges at *ca.* 284.5 eV and 400 eV corresponding to the C and N K-shells (Fig. 3). A splitting in the π^*-*type* peak of the nitrogen K edge exhibits two features at *ca.* 398.7 and 400.7 eV, corresponding to highly coordinated N atoms replacing C atoms within the graphene sheets (*ca.* 401 - 403 eV), and pyridinic nitrogen (*ca.* 399 eV).

It is important to note that, as the *overall* N content increases within these structures, the number of graphitic walls within the nanofibers decrease and the proportion of pyridine-like N also increases (remaining almost constant the number three coordinated N atoms). Therefore, these pyridine-like N sites "cavities" or "edges" within the predominantly graphitic framework are responsible for the roughness and for interlinked morphologies observed in these doped nanostructures

These N-doped fibers are expected to be metallic, and may exhibit stable field emission properties at low voltages (*e.g.* < 0.2 kV). Since these 'hollow' fibers do not easily break upon bending, they may well behave as shock absorbing fillers in the fabrication of robust composites.

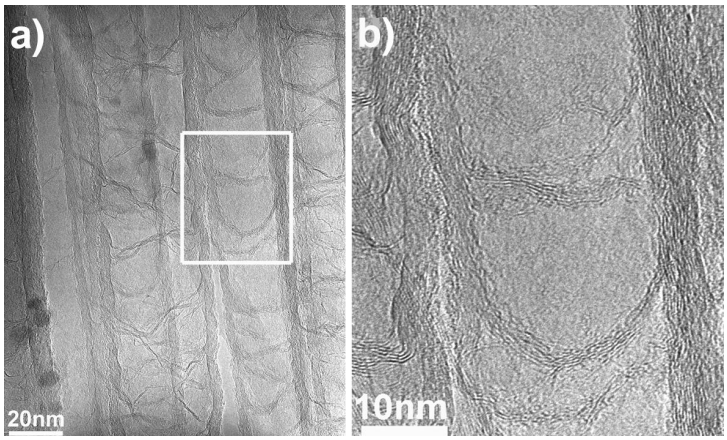

FIGURE 2. (a-b) TEM and HRTEM images of an aligned bundle of CN_x nanotubes, exhibiting corrugation, inter-linkage and compartments within an individual N-doped tubule.

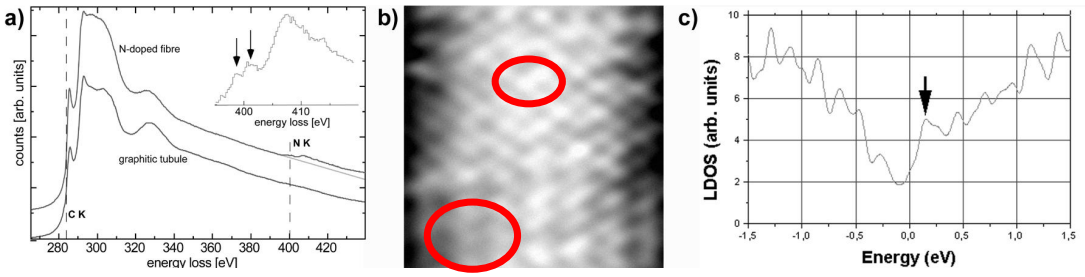

FIGURE 3. (a) EEL spectra of a typical C_xN_y nanofiber, suggesting an sp^2 graphite-like network due to the presence of the well defined σ^* and π^* features. Inset shows a splitting in the π^* of the N K-shell due to two different types of bonds (two and three coordinated N); (b) Atomic resolution STM image of a small area on the surface of a 20 nm diameter nanotube exhibiting distortions and holes (circles) caused by the presence of pyridine-like islands; (c) Tunneling spectra acquired on a straight section of an N-doped carbon nanotube, exhibiting a prominent donor peak close to the Fermi level.

Figure 3c exhibits an ST spectrum recorded within a straight section of the N-doped carbon nanotube. For pure carbon nanotubes, the valence and conduction band features appear to be symmetric about the Fermi level [20], while for the N-doped tube (Fig. 3c) an additional electronic feature occurs at *ca.* 0.18 eV. This result is in contrast to the B-doped case [21] where variations in the peak position are observed due to the formation of local

phases, suggesting that the N is distributed along the nanotube with small variations in the N concentration. The presence of an electronic states at the Ef indicates that the N-doped material may indeed be metallic. It is noteworthy that the electron donor feature observed in the N-doped material is always seen along the nanotubes.

We performed *ab-intio* calculations using local density approximation of density functional theory, in order to simulate more accurately the doping effect on graphene planes. [20]. In this context, we calculated a 3 x 3 graphite unit cell in which one of the 18 C atoms was replaced by a N (*ca.* 5.5% N content). We observed that this individual N is responsible for an increase of the Fermi energy by *ca.* 1.21 eV. We also noted the presence of states in the conduction band (above the Fermi level [20]). In addition, these donor states are completely delocalized over several angstroms due to the original metallic behavior of the un-doped graphene sheets.

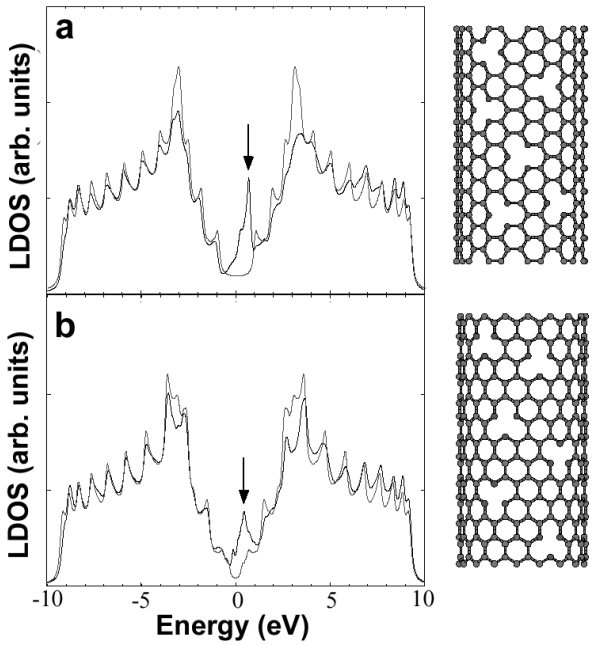

FIGURE 4 Theoretical LDOS associated with a Pyridine-like structure with N-doping carbon nanotubes displaying (a) armchair (10,10) and (b) zigzag (17,0) configurations. In both cases, N atoms were placed randomly (N: red spheres – C: blue spheres; right hand images). The LDOS of doped (black curve) and pure (red curve) carbon nanotubes are compared. It is clear that pyridine-like sites are responsible for the prominent donor-like features (shown by arrows in the conduction band) close-above the Fermi energy. Note that the semiconducting (zigzag) nanotube becomes metallic after introducing N in the carbon lattice.

Due to the presence of pyridine -like sites, observed by EELS and XPS, we carried out tight binding calculations using a recursion approach [20], which has been successful in calculations carried out for $B_xC_yN_z$ nanotube heteojunctions [20]. In particular, we analysed the DOS associated with the N atoms arranged in a pyridinic fashion, randomly distributed within armchair and zigzag carbon nanotubes. The corresponding DOS for both types of chiralities are depicted in Fig. 4. Here, we observed prominent donor peaks close-above the Fermi energy (at *ca.* 0.2 eV), which are in good agreement with the experimental data obtained using STS (Fig. 4). Thus, N doping, using pyridine-type units within carbon tubes, are responsible for a strong related π peak (shown by arrows in the black curves of Fig. 4) in the conduction band of the original undoped carbon nanotube (red curves, Fig. 4).

3. B-doped Carbon Nanotubes

Long B-doped carbon nanotubes (≤ 100μm) are obtained when arcing BN/graphite electrodes in a He or N_2 atmosphere. The products also contain hemitoroidal nanotube caps, nanofibres and polyhedral particles. Surprisingly, ill-formed caps, occasionally open or exhibiting negative curvature regions (Fig. 5) [22], are also observed with higher B concentrations at their ends (revealed by EELS analyses). This suggests that boron act as catalyst in the formation of long tubules. However, careful EELS studies have shown that only minute B traces (<1 %) are present within the tubules (not shown here).

Electron diffraction (ED) studies have shown that these long B-doped carbon nanotubes exhibit a preferred *zigzag* or *near zigzag* chirality (*e.g.* zigzag ± 3°) [23]. Chiralities corresponding to the armchair configuration are rarely observed and other helical arrangements are never dominating. In this context, we have performed static and dynamic *ab-intio* calculations, demonstrating that boron indeed acts as a surfactant during the growth of long tubes [23, 24]. This growth model only applies to zigzag tubules (Fig. 6), implying that this nonchiral geometry should be favored in B-doped nanotubes, which also exhibit a high aspect ratio.

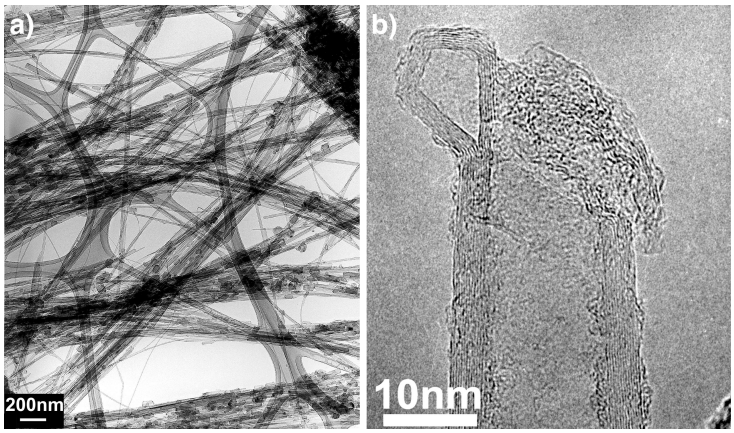

FIGURE 5. (a) Low magnification TEM image of B-doped carbon nanotubes produced by the arc discharge technique, note that the amount of polyhedral particles is significantly reduced; (b) HRTEM image of an ill-formed nanotube cap in which one segment of the tube is closed adopting a diamond-like shape, whereas the other end remained open exhibiting amorphous material around the tip.

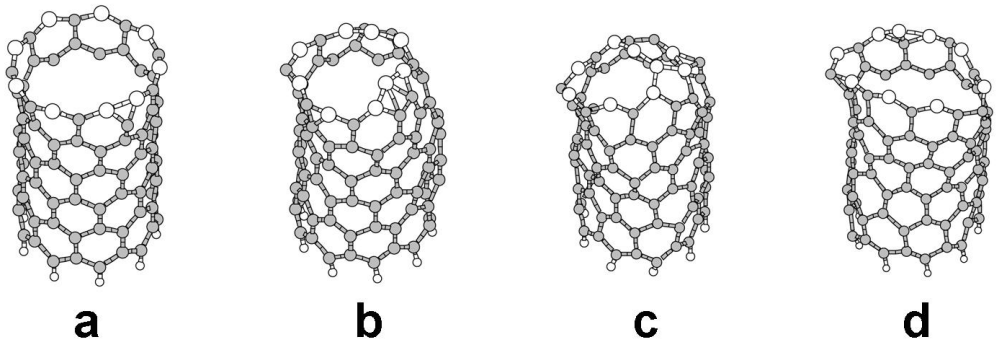

FIGURE 6. Molecular models of a B-doped C(9,0) nanotube. In (a), the ground state geometry at T=0 K is represented; (b), (c), and (d) three different snapshots for the doped nanotube at 2500 K. Snapshot (d) represents the final configuration reached by the system at the end of the Molecular Dynamics (MD) run. (a) [23].

In order to understand the growth of long B-doped carbon nanotubes, we performed *ab-intio* molecular dynamics (MD) calculations on a B-doped (9,0) tube [23]. It was observed that at 500 K, B atoms dimerise (Fig. 6a). However, at 2500 K, B trimers are formed, followed by the appearance of B-B-B- C-C and C pentagons at the tip of the nanotube (Fig. 6b). At this point, the formation of pentagons induced curvature and causes a bending at the edge structure, rapidly leading to partial closure. However, in contrast with the pure carbon nanotube case, where the bridging quickly led to tip closure into

a defected graphitic dome, here the B-B bonds easily break, and the tip structure of the doped tube reopens. (Fig. 6d). Therefore, B atoms located at the tip of growing zigzag nanotubes act against tube closure [23-24]. This result explains the increased length of zigzag B-doped carbon nanotubes observed experimentally. In a further simulation on a C (5,5) tube closed by the B-doped hemisphere, cap reopening was not observed during 10 ps of simulations at 3000 K. The latter suggests that long carbon nanotubes will preferentially grow in a zigzag configuration when B is used as a dopant [23-24].

Microwave conductivity measurements revealed that B-doped carbon nanotubes are intrinsically metallic [10], thus differing from standard pure carbon nanotubes, which show thermally -activated transport. Carroll, *et al.* [21] detected characteristic peaks in the density of states (DOS) using scanning tunneling spectroscopy (STM). The peaks appeared in the valence bands caused by the introduction of BC_3 islands (which acts as an acceptor) in the carbon lattice [21]. The results were confirmed using *ab-intio* calculations, indicating that the changes in the electronic structure are mainly due to the presence of dopant rich islands and not to isolated substitutional boron atoms [21].

4. Connecting SWNTs

Samples of SWNTs were produced using the arc discharge technique involving Ni-Y-graphite electrodes [25]. One mg. of the tube material was dispersed ultrasonically in 10 ml ethanol for one minute and a few drops of the suspension were deposited onto holey carbon grids for transmission electron microscopy observations. The experiments were carried out in a high-voltage Atomic Resolution Transmission Electron Miscroscope (ARTEM) with accelerating voltage of 1.25 MeV (JEOL-ARM 1250, located at the Max-Planck-Institut für Metallforschung in Stuttgart). Observations were performed at specimen temperatures of 800 °C using a GATAN heating stage. Images were recorded with a slow-scan CCD camera. The nanotube behaviour was monitored under electron irradiation of standard imaging conditions (1.25 MeV electron energy and beam intensity of *ca.* 10 A/cm^2).

From the random criss-crossing distribution of individual nanotubes and nanotube bundles on the specimen grid, several contact points could be

identified where tubes were crossing and "*touching*" each other. These arrangements were picked and observed under electron beam exposure. After a few minutes of irradiating two crossing tubes (Fig. 7a), their merging was observed at the point of contact, resulting in the formation of a junction with an "X"-shape (Fig. 7b). In other words, the tubes were welded together under the influence of electron irradiation and annealing at their contact region [26-27]. During the junction formation, the upper "arms" of the "X"-junction cross over and protrude out of the plane [27]. From our direct observations, we conclude that it is possible to join two SWNTs of different diameter perfectly through the formation of a stable junction. In certain cases, the geometry of the junctions is difficult to visualize from the projected images, but junctions such as "X", "Y" and "T" can be well documented.

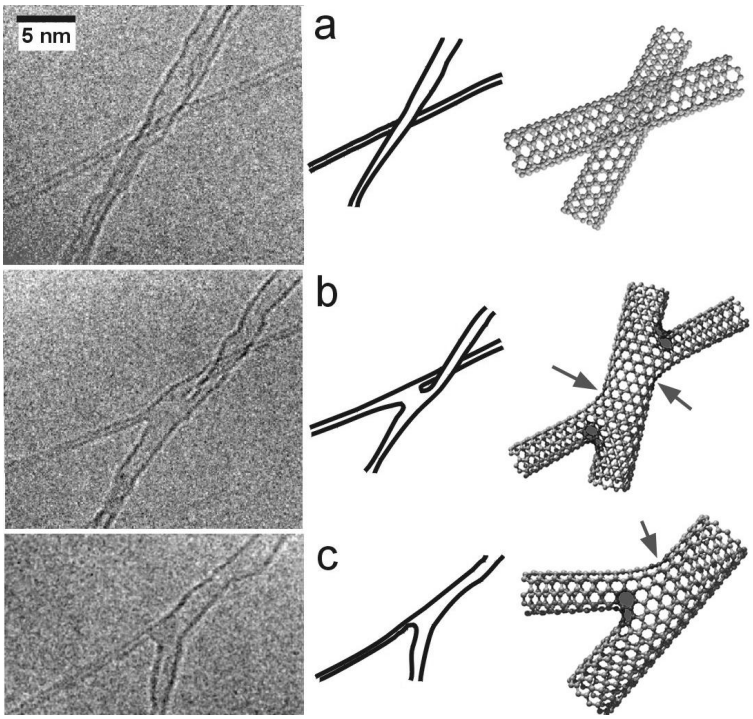

FIGURE 7. a) A SWNT of *ca.* 2.0 nm (running from bottom-left diagonally towards top right) crossing with an individual SWNT of ca. 0.9 nm. Note that the crossing tubes exhibit similar contrast, thus indicating that they may be "touching"; (b) After 60 seconds, electron irradiation promotes a molecular connection between the thin and the wide diameter tube forming an "X" junction (Fig. 1b). Schematics are shown below in order to show that this junction is twisted out of the plane; (c) subsequent electron irradiation of the structure promotes breakage of the thin tube (5 Å diameter). The resulting structure now constitutes a "Y" junction. Note that the junction clearly exhibits tubes of different diameters molecularly joint. Molecular models of each image are also provided and heptagonal ring are indicated in red [27].

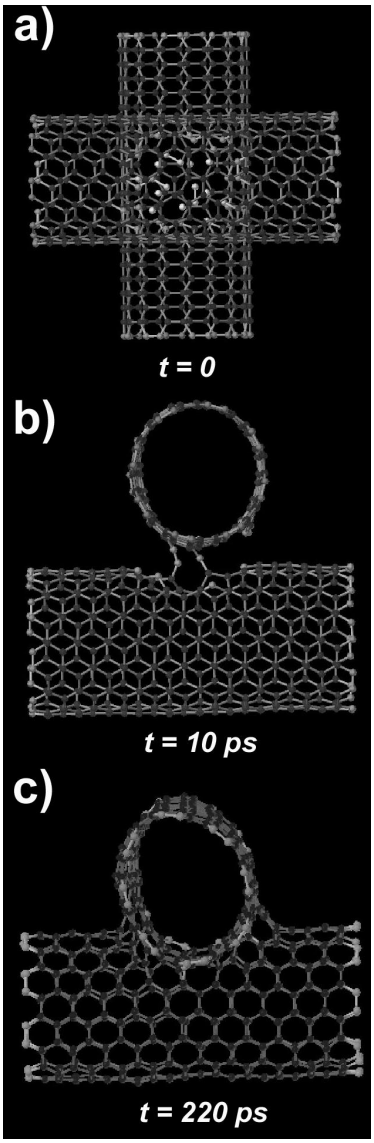

FIGURE 8. TBMD simulations at 1000 °C of two crossing (8,8) carbon nanotubes (diameter *ca.* 1.1 nm), which transform into an individual molecular "X" junction: **(a)** The two crossing tubes contain 20 vacancies on their surfaces, concentrated in the neighboring site, so that a connection can be promoted (top view). This unit cell contains 860 carbon atoms (white, yellow, green, blue and red spheres, illustrating an atomic coordination of 0, 1, 2, 3, and 4, respectively). Periodic boundary conditions are imposed along both nanotube axes and the time steps of 0.7 fs were monitored as for the previous case (Fig. 4); **(b)** After 10ps, two links between the two defected carbon structures are formed via carbon chains (side view); **(c)** After 220ps, a surface reconstruction occurs and the resulting structure consists of a molecular "X" junction. This reconstructed surface mainly contains sp^2 carbon atoms, and exhibit six heptagons, one octagon, one pentagon and two dangling bonds.

The "X"-junction shown in Fig. 7a evolves, when exposed to sustained electron irradiation. It has been established from earlier work [26] that continuous sputtering of carbon atoms takes place from the nanotube body during irradiation, leading to dimensional changes, surface reconstructions and breakage. In the case of the junction here, it leads to a breaking of one of the "arms" within the junction. At this point, the first arm of the junction (usually the thinnest in this case of *ca.* 5 Å) gets pinched off, and the geometry becomes a threefold junction with a "Y"-shape (Fig. 7c). This suggests that controlled electron irradiation can be used to tailor the transformation of the junction geometries which may be used in order to generate "nano-devices" with three, four or more terminals. It needs to be pointed our that the angle between the tubes cannot be measured directly here because we obtain only a projection of the junction in the image plane.

In order to explain the connection process, we carried out another TBMD simulation of two crossing tubes at 1000 °C, which resulted in the creation of an almost perfect molecular junction (Fig. 8). Twenty atoms (Fig. 8) were removed randomly from the lattices of the two crossed nanotubes, thus creating vacancies (dangling bonds) in the crossing region. After 10 ps., the crossing tubes approach each other and the dangling bonds start connecting through carbon chains (Fig. 8). After 220 ps, a complete surface reconstruction takes place, leading to the creation of a molecular "X" junction, mainly exhibiting sp^2-carbon atoms (Fig. 8). Both heptagons and octagons are observed on the reconstructed surface. The key role played by these defects is certainly to increase the energetic stability of the structure when compared to that shown in Fig. 8b, as well as to introduce a smooth negative curvature in both hexagonal carbon networks. The present simulation provides a clear picture of an intermediate state of the "welding" process.

The latter process witnessed in Fig. 7 clearly indicates that it is possible to connect crossed SWNTs in order to create molecular junctions experimentally, which could be used in the fabrication of three and four terminal transistors. In this context, we propose that high energy irradiation at high temperatures (700 – 1000 °C) could be used to weld crossed SWNTs, thus resulting in the formation of "X", "T" and "Y" molecular carbon junctions. Therefore, we envisage that the formation 2D and 3D SWNT networks could be achieved when localized irradiation at elevated temperatures is applied to arrays of crossed SWNTs. The production of these novel carbon-carbon

nanocomposites would certainly revolutionize specific areas in electronics (*e.g.* formation of memory devices and circuits using 2D SWNT matrices) and materials (*e.g.* creation of extra-light and super-robust fabrics using 2D and 3D SWNT networks).

5. Conclusions

It is now possible to produce n-type and p-type carbon nanotubes using nitrogen, and boron as doping agents respectively. The tubes have been synthesised by thermolytic processes using the Pyrolysis of ferrocene/melamine mixtures, and the arc discharge of B-graphite electrodes in inert atmospheres. It is envisaged that the formation of n-p junctions, using N- and B-doped carbon nanotubes respectively, may play a key role in the fabrication of novel carbon-based electronic devices. We have also observed (in-situ) the formation of molecular carbon nanotubes junctions under high electron irradiation at high temperatures. In this context, we have elucidated the mechanism whereby nanotubes merge, thus forming junctions. This phenomenon consists of the creation of vacancies, which trigger the reconstruction of the tube surfaces. The latter result implies that it should be possible to fabricate carbon tube networks, which will certainly revolutionise key areas in nanotechnology.

Acknowledgements

We thank CONACYT-México grants: W-8001-millennium initiative, G25851-E, 37589-U, 36365-E (HT, MT), the DFG grant Ru342/11-2 (NG), The Belgian interuniversity project (PAI P4/10) and the European Union: COMELCAN project contract N° HPRN-CT-2000-00128 (JCC), NANOCOMP HPRN-CT-2000-00037 (NG), and CNT-NET project contract N° G5RT-CT2001-05026 (MT), for financial support. We are in debt to F. Phillipp and R. Höschen for the hospitality, assistance and facilitating the use of the electron microscope based in Stuttgart. PMA acknowledges funding from Office of Naval Research and the focus center for Interconnects at Rensselaer Polytechnic Institute.

References

1. Kroto, H. W., Heath, J. R., O'Brien, S. C., Curl, R. F., Smalley, R. E. *Nature* **318**, 162 (1985).
2. Iijima, S. *Nature* **354**, 56 (1991).
3. Endo, M. & Kroto, H.W. *J. Phys. Chem.* **96**, 6491 (1992).
4. Dresselhaus, M.S., Dresselhaus, G., Eklund, P.C. (1996) Science of Fullerenes and Carbon Nanotubes, Academic Press, New York.
5. Endo, M., et. al. *J. Phys. Chem. Solids* **54,** 1841-1843 (1993).
6. Amelinckx, S., et. al. *Science* **265,** 635 (1994).
7. Terrones, M., et. al. *Nature* **388**, 52 (1997).
8. Thess, A., et. al. *Science* **273**, 483 (1996).
9. Hsu, W.K., Hare, J.P., Terrones, M., Harris, P.F.J., Kroto, H.W., Walton, D.R.M. *Nature* **377,** 687 (1995).
10. Terrones, M., Hsu, W. K., Kroto, H. W., Walton, D. R. M. (1998) Nanotubes: A revolution in material science and electronics". In *Fullerenes and Related Structures;* Topics in Chemistry Series, Ed. A. Hirsch (Springer-Verlag), vol. 199, ch. 6, pp.189-234.
11. Ajayan, P.M. & Ebbesen, T.W. *Rep. Prog. Phys.* **60**, 1025 (1997).
12. Dresselhaus, M.S., Dresselhaus, G., Avouris, P. *In Carbon Nanotubes.* Top. Curr. Appl. Phys. Vol. **80**, pp. 1-325 (2001).
13. Yao, Z., Postma, H.W.C., Balents, L., Dekker, C. *Nature* **402**, 273 (1999).
14. Chernozatonskii, L.A. *Phys. Lett. A* **172**, 173 (1992).
15. Scuseria, G.E. *Chem. Phys. Lett.* **195**, 534 (1992).
16. Treboux, G., Lapstun, P., Siiverbrook, K. *Chem. Phys. Lett.* **306**, 402 (1999).
17. Menon, M., Srivastava, D. *Phys. Rev. Lett.* **79,** 4453 (1997).
18. Andriotis, A.N., Menon, M., Srivastava, D., Chernozatonskii, L.A. *Phys. Rev. Lett.* **87**, 6802 (2001).
19. Terrones, M., et. al. *Appl. Phys. Lett* **75**, 3932 (1999).
20. Czerw, R., et al. *Nanoletters* **1**, 457 (2001).
21. Carroll, D.L., et al. *Phys. Rev. Lett.* **81**, 2332-2335 (1998).
22. Terrones M, Hsu WK, Ramos S, Castillo R, Terrones H. *Ful.l Sci. & Tech.* **6**, 787 (1998).
23. Blase, X., et. al. *Phys. Rev. Lett.* **83**, 5078-5081 (1999).
24. Hernández, E. Ordejon, P., Boustani, I., Rubio, A., Alonso, J.A. *J. Chem. Phys.* **113** 3814 (2000).
25. Journet, C., et. al. *Nature* **388**, 756 (1997).
26. Terrones, M., Terrones, H., Banhart, F., Charlier, J.C., Ajayan, P.M. *Science* **288**, 1226 (2000).
27. Terrones, M, Banhart, F., Grobert, N., Charlier, J.-C., Terrones, H., Ajayan, P.M. *Phys. Rev. Lett.* **89**, 75505-8 (2002).